Supporting Information

Hysteresis of a Tension-Sensitive K^+ Channel Revealed by Time-Lapse Tension Measurements

Masayuki Iwamoto[1*] & Shigetoshi Oiki[2*]

[1]Department of Molecular Neuroscience, University of Fukui Faculty of Medical Science, 910-1193 Fukui, Japan
[2]Biomedical Imaging Research Center, University of Fukui, 910-1193 Fukui, Japan

[*]Correspondence to: iwamoto@u-fukui.ac.jp and oiki-fki@umin.ac.jp

This PDF file includes:

Materials and Methods

Reagents

Azolectin (L-α-phosphatidylcholine type IV-S) was purchased from Sigma-Aldrich (St. Louis, MO, USA). Other chemicals were purchased from Nacalai Tesque (Kyoto, Japan).

Sample preparation

Expression and purification of the E71A mutant of the KcsA channel are described elsewhere[1,2]. Liposomes and channel-incorporated liposomes (proteoliposomes) were prepared following a previous report[3] with modification. Two hundred microliters of a 10 mg/ml chloroform solution of azolectin was dried in an eggplant flask under N_2 gas flow to form a thin lipid film. One milliliter of 200 mM KCl solution was added to the flask and sonicated using a bath sonicator (Model 1800, Branson, Danbury, CT, USA) to obtain a multilamellar liposome suspension (2 mg/ml). The suspension was passed through a polycarbonate membrane (pore size, 100 nm) eleven times using an extruder (Mini-Extruder, Avanti Polar Lipids, Alabaster, AL, USA) to obtain unilamellar liposomes. The purified channel proteins were incorporated into the liposomes by the dilution method[3] with a lipid-protein weight ratio of 2000. The proteoliposome suspension was mixed with a small amount of concentrated buffer (pH 7.5 or 4.0) immediately before the single-channel current measurements.

Experiments for measurement of the bilayer tension using the CBB

The experimental setups for the CBB were the same as those previously reported[3–5] except for the pressure measurement system. The equilibrium bilayer tension was previously evaluated using the other method (see Figure S3)[3], which provides an estimate of the intra-bubble pressure in the range of several tens of *Pa* to over 100 *Pa*. The used fine pressure gauge (DP103; Validyne Engineering, Los Angeles, CA, USA) covers the relevant pressure range measurements. The pressure gauge was connected to a glass pipet holder, and the pressure was continuously monitored via a signal amplifier (PA701; Krone, Tokyo, Japan).

The intra-bubble pressure was measured with an atmospheric pressure reference, and care had to be taken in defining the null pressure. A glass pipet (ID/OD, 1.05/1.5 mm; tip diameter, 50 μm) was set in a micropipet holder with a pressure port, which was connected to the motor-driven micro manipulator (EMM; Narishige, Tokyo, Japan) on the stage of an inverted microscope (IX73; Olympus, Tokyo, Japan). The glass pipet tip was immersed into the liposome (or proteoliposome) suspension solution with the pressure port open. The aqueous solution moved up into the pipet by capillary action. A trick of the method is to allow the capillary action to proceed for minutes until the solution reaches the equilibrium level, at which the hydrostatic pressure and the capillary action are balanced. In the pipet, an Ag/AgCl electrode tip is advanced to 3 mm from the capillary tip beforehand. Thus, the solution reaches the electrode through capillary rise, ensuring electric connectivity. Then, the tip of the pipet is soaked in an oil (hexadecane) phase at depth for the following experiments (~100 μm). The meniscus at the tip remained there, indicating that additional hydrostatic pressure in the oil phase is negligible. The pressure line is closed, and the intra-bubble pressure is defined as zero.

Using the pneumatic manipulator (IM-11-2; Narishige, Tokyo, Japan), the liposome (or proteoliposome) suspension was swollen from the tip of the pipet, forming a water-in-oil bubble lined with a lipid monolayer. A lipid bilayer (CBB) was formed by contacting two bubbles. Under visual inspection, the size of the bubbles was maintained by fine-tuning the injectors, such that abrupt and large operations are avoided. Electrical recordings were performed using an

amplifier (EPC800; HEKA, Lambrecht/Pfalz, Germany), and microscope images were recorded with a digital camera (ORCA-Flash2.8; HAMAMATSU, Hamamatsu, Japan).

Evaluation of the bilayer tension

The shape of the bubble is spherical at equilibrium since gravity has a negligible influence on small-sized bubbles (R < 50 μm). From the time-lapse bubble images, the radius and contact angle for each bubble were evaluated using the image analysis method (Figure 1). In the image analysis, the bubble images were fitted to ellipses using data analysis software (Origin Pro; OriginLab, Northampton, MA, USA), and the intersections of two ellipses were solved using a free computer algebra system (wxMaxima, Maxima.sourceforge.net). The geometric parameters R_1 and R_2 represent the principal radii of curvature of the bubble. The images are sampled mostly at 1 Hz, and the continuously measuring pressure data at the instance of the image sampling are retrieved. Accordingly, with the pressures, the monolayer tension γ_{mo} was obtained from the Young-Laplace equation $\gamma_{mo} = R_1 R_2/(R_1 + R_2)\,\Delta p$. Then, from the contact angle θ, the bilayer tension γ_{bi} was calculated from the Young equation, $\gamma_{bi} = \gamma_{mo-L}\cos\theta_L + \gamma_{mo-R}\cos\theta_R$, where L and R indicate the left and right bubbles, respectively.

Evaluation of the tension - P_{open} relationship

Single-channel current traces with several active KcsA channels (Figure 3C) were first digitalized as discrete current levels (how many channels are active; Figure S5B) using the event detector (Clampfit, Molecular Device, San Jose, CA, USA). Every 100 ms, the digitalized current levels were integrated for a defined interval, t_{int}, such that $\int_{t-tint/2}^{t+tint/2} i\,dt$. This discrete probability distribution was fitted with the binomial distribution, and the P_{open} values are thus obtained every 100 ms. The image sampling frequency was mostly 1 Hz, and the geometrical parameters, such as the principal radii for both bubbles and the contact angle, are obtained using the image analysis off-line. At every 100 ms, the pressure values at the instance of the image capture time and the P_{open} at the nearest neighbor of the image capture time were retrieved, and the bilayer tension was calculated using the Young-Laplace and Young principles. The potential error of synchronization of P_{open} data less than 50 ms was ignored because the interval, t_{int}, for calculating the P_{open} was longer than 50 ms, mostly 500 ms.

Electrophysiological recordings

Membrane electrical features, such as the membrane capacitance and resistance, were recorded by applying ramp potentials of ±10 mV and analyzed using software (pCLAMP; Molecular Devices). From the image-analyzed membrane area, the specific membrane capacitance was evaluated. For the channel activity measurements, channel-containing proteoliposome suspension was swelled to form the bubble. Some of the channel molecules are spontaneously incorporated into the CBB and exhibit a single-channel current. The single-channel current resolvable traces of the non-inactivating E71A mutant KcsA channel were recorded under a constant V_m of +100 mV, while Δp was arbitrarily manipulated during the recording. For the time course of P_{open}, the single-channel current traces were analyzed every 1 sec. From the current histogram, P_{open} was calculated using the binomial distribution.

Statistical Analysis

Average values are expressed as means ± SEM. For comparison of means between categories, Welch's *t* test (two tailed, no assumption of variance) was carried out, and *P* values were obtained from a *t*-value lookup table.

Supplementary Text

The Young-Laplace principle for a single bubble

In the CBB, the intra-bubble pressure of both sides is continuously monitored. γ_{mo} as a function of p is shown for the left and right bubbles (Figure S1A). The relation is nearly linear, but the pressure-increasing and -decreasing phases exhibit different slopes. This raises the question of an apparent hysteresis in the p-γ_{mo} relationship. However, this is not the case. The trajectories are projected onto the Young-Laplace plane in the three-dimensional plot given the measured radii (Figure S1B). As the pressure increases, the bubble size increases, and the trajectory moves on the surface, exhibiting a steeper slope.

In addition to nearly linear relationships of the p and γ_{mo}, the bilayer tension is linearly related to the monolayer tension (Figure 2C). Thus, trends of the pressure values serve as a benchmark for manipulating the pressure injector to control the bilayer tension.

Lipid partitioning to the oil-water interface

The time course of lipid partitioning to the oil-water interface can be examined using time-lapse measurements of the monolayer tension (Figure S2). Under visual inspection, the size of a single bubble is maintained nearly constant through injector manipulation, while the pressure is continuously measured. The monolayer tension is evaluated from the radius and pressure. This approach is similar to a pendant-drop method[6] but is distinct in the following respects. First, the bubble size is small (<100 μm in diameter), and the gravity effect is negligible, and the bubble is spherical. Second, the water flow in and out of the bubble is negligible since the bubble size is maintained nearly constant.

The time course of the monolayer tension (Figure S2) indicates that lipid partitioning reaches equilibrium very slowly (time constant: 20 s), consistent with previous reports[7]. Accordingly, upon applying a pressure, γ_{mo} immediately increases before partitioning of phospholipids to the bubble expanded surface.

Comparison of the bilayer tension at equilibrium with that from the previous method

The bilayer tension evaluated by the bubble shape-pressure method is compared with that evaluated by the previous method using voltage steps under the Young-Lippmann principle[3,8].

In the previous method, changes in the bilayer tension and the contact angle at different membrane potentials are exploited (electrowetting, Figure S3A). The Young-Lippmann principle is

$$\cos\theta_0 - \cos\theta_V = \frac{C_M}{4\gamma_{mo}} V_m{}^2 \qquad \text{(Eq. S1)},$$

where θ_0 and θ_V represent the contact angles under the membrane potentials of 0 and V mV, respectively, and C_M is the specific membrane capacitance. Step potential changes are imposed successively, during which the contact angle is evaluated for each voltage (Figure S3). Several seconds are needed to complete the step potential protocol, and the evaluation is at equilibrium in nature.

The two methods were applied in parallel to the same lipid bilayer, and the evaluated γ_{bi} values are shown in Figure S3B. The results show comparable bilayer tension values; the correlation coefficient is 0.95, and the slope of the linear regression (broken red line) is 0.89. The agreement of the bilayer tension values evaluated using the two independent methods rationalizes the bubble shape-pressure method, in which measurements of the intra-bubble pressure were fine tuned.

Dynamic responses of the bubble shape-pressure system

The bubble shape in CBB is equilibrated in free space (hexadecane) and subject to transition upon physical perturbations, such as pressure and voltage changes. The response time of the CBB represents the transition time for another equilibrium. The bubble shape-pressure method has two independent classes of measurements: bubble pressure and geometry. The two classes are synchronized in the recording, but each class exhibits specific responses in its time course, leading to potential errors in the bilayer tension evaluation in non-equilibrium conditions. The objective of the following experiments is to estimate the response time of the bilayer tension upon application of membrane potential and pressure via monitoring directly measurable parameters, the contact angle. Here, the experiments were performed with a sampling frequency of 10 Hz.

The membrane potential vs. the contact angle.

Application of membrane voltage squeezes the bilayer thickness (electrostriction; $1/2\ CV^2$), leading to decreased bilayer tension and increased contact angle (Eq. S1). Under the voltage-clamp condition, the membrane potential is rapidly changed, and changes in the contact angle indicate the system's dynamic response. In the CBB, the series resistance as low as 600 kΩ allows a much faster voltage-clamp than usual patch-clamp methods. In parallel to changes in the contact angle, the bilayer area changes, known as the electrowetting[8]. Changes in the contact area and angle are well established in the electrowetting phenomenon, and underlying physical processes have been elucidated. In the DIB, changes in the bilayer area are known as zipping (increasing the bilayer area upon application of voltage) and unzipping (decreasing the bilayer area upon less voltages)[9].

Step voltage changes to +200 mV were repeatedly applied, and the contact angle changed reversibly (Figure S4). The contact angle increases upon a voltage jump to +200 mV and decreases upon returning to 0 mV. A time course of the contact angle is shown for +200 mV step changes and their return to 0 mV (Figure S4A, B), which was fitted with an exponential function ($f(t) = c + a \exp[-t/\tau]$). The time constant ($\tau$) of the zipping process was slower than unzipping ($t_{zip} = 187.4 \pm 12.8$ ms, $t_{unzip} = 109.7 \pm 9.0$ ms).

As expected, the pressure never changed upon voltage steps (Figure S4C). Accordingly, the bilayer tension follows the time course of the contact angle (Figure S4D,E).

In the response of the contact angle to the voltage steps, the difference in the time course is apparent for the voltage application and return. The time constant of the contact angle is substantially shorter for the return potential, shared with the time course of bilayer area changes (Figure S4F). Squeezing the bilayer thickness under the voltage (electrostriction) renders the bilayer area expanded, known as electrowetting[14] or zipping[9]. As the bilayer is zipping, the organic solvent must be excluded from regions of approaching monolayers, and the viscous drag of solvent retards the process. In the unzipping process without viscous drag, the time course was

faster than zipping. Noted are faster zipping and unzipping than previous reports simply because of the bubbles and bilayer's small size [30,31].

The response time of the contact angle change upon voltage steps represents experimental verification of the system's dynamic response. The result indicates that bilayer tension changes completed with the time constant of ~150 ms, which is rapid enough to trace tension-dependent channel activity at 1 Hz.

The real intra-bubble pressure

The potential pressure gradient between the intra-bubble pressure and the measured pressure is determined by the medium flow velocity based on Bernoulli's principle. Representative data of the volume of a bubble and its change under step pressure application are shown in Figure 4B. The volume change starts at the upstroke of the pressure change and gradually continues. The maximum rate of volume change is 0.3 pL/ms. Given one pL/ms as the upper limit of the volume change rate, the flow velocity is calculated as 0.796 mm/s across the pipet tip of 20 μm in radius. Based on the Bernoulli principle ($v^2/2 + p/\rho$ = constant, where v is the velocity and ρ is the density), the pressure difference in the bubble is 0.733 m*Pa*. Accordingly, the experimental error in evaluating the intra-bubble pressure is negligible.

Arguments of the pressure gradient in the measurement system are shared with those in the classical physicochemical measurement of monolayer tension using the maximum bubble pressure method[10]. A pressure gradient across the pipet and the bubble occurs under rapid gas flow. This issue is analogous to voltage errors of the membrane potential under the voltage-clamp condition, named the series-resistance error[11]. This error is remedied by using low-resistance pipets and supercharging of the applied voltage[12]. In the bubble shape-pressure method, a large-bore (~50 μm in diameter) pipet is used, and the pressure gradient is minimized by slowly changing the pressure, leading to a negligible pressure gradient.

An analysis example for tension-P_{open} relationships

An example analysis for calculating P_{open} values relating to the bilayer tension are shown for representative data (Figure S5). The current traces (Figure S5A) were digitalized as discrete current levels (Figure S5B). Every 100 ms, the digitalized current levels were integrated for t_{int} of 250 ms. The probability distribution for current levels was fitted with the binomial distribution (Figure S5C), and the P_{open} is thus calculated every 100 ms (Figure S5D). From the images of bubbles with the image sampling frequency of 1 Hz, the principal radii for both bubbles and the contact angle are obtained. Pressure values at the instance of the image capture time were retrieved, and the bilayer tension was calculated (Figure S5E). Similarly, the P_{open} value at the nearest neighbor of the image capture time was retrieved to obtain the tension-P_{open} relationships.

Crystal structures of the KcsA channel in different conformations

Crystal structures of the KcsA channel with different conformations are shown in a conventional style (Figure S6), rather than the schematic representation shown in Figure 5D.

References

(1) Iwamoto, M.; Shimizu, H.; Inoue, F.; Konno, T.; Sasaki, Y. C.; Oiki, S. Surface Structure and Its Dynamic Rearrangements of the KcsA Potassium Channel upon Gating and

Tetrabutylammonium Blocking. *J. Biol. Chem.* **2006**, *281* (38), 28379–28386. https://doi.org/10.1074/jbc.M602018200.
(2) Iwamoto, M.; Oiki, S. Amphipathic Antenna of an Inward Rectifier K+ Channel Responds to Changes in the Inner Membrane Leaflet. *Proc. Natl. Acad. Sci. U. S. A.* **2013**, *110* (2), 749–754. https://doi.org/10.1073/pnas.1217323110.
(3) Iwamoto, M.; Oiki, S. Constitutive Boost of a K+ Channel via Inherent Bilayer Tension and a Unique Tension-Dependent Modality. *Proc. Natl. Acad. Sci. U. S. A.* **2018**, *115* (51), 13117–13122. https://doi.org/10.1073/pnas.1812282115.
(4) Iwamoto, M.; Oiki, S. Contact Bubble Bilayers with Flush Drainage. *Sci. Rep.* **2015**, *5*, 9110. https://doi.org/10.1038/srep09110.
(5) Iwamoto, M.; Oiki, S. Lipid Bilayer Experiments with Contact Bubble Bilayers for Patch-Clampers. *J. Vis. Exp.* **2018**.
(6) de Gennes, P.-G.; Brochard-Wyart, F.; Quere, D. *Capillarity and Wetting Phenomena: Drops, Bubbles, Pearls, Waves*; Springer, 2003.
(7) Venkatesan, G. A.; Lee, J.; Farimani, Amir Barati Heiranian, M.; Collier, C. P.; Aluru, N. R.; Sarles, S. A.; Farimani, A. B.; Heiranian, M.; Collier, C. P.; Aluru, N. R.; Sarles, S. A. Adsorption Kinetics Dictate Monolayer Self-Assembly for Both Lipid-In and Lipid-Out Approaches to Droplet Interface Bilayer Formation. *Langmuir* **2015**, *31* (47), 12883–12893. https://doi.org/10.1021/acs.langmuir.5b02293.
(8) Taylor, G. J.; Venkatesan, G. A.; Collier, C. P.; Sarles, S. A. Direct in Situ Measurement of Specific Capacitance, Monolayer Tension, and Bilayer Tension in a Droplet Interface Bilayer. *Soft Matter* **2015**, *11* (38), 7592–7605. https://doi.org/10.1039/C5SM01005E.
(9) Najem, J. S.; Freeman, E. C.; Yasmann, A.; Sukharev, S.; Leo, D. J. Mechanics of Droplet Interface Bilayer "Unzipping" Defines the Bandwidth for the Mechanotransduction Response of Reconstituted MscL. *Adv. Mater. Interfaces* **2017**, *4* (3), 1600805. https://doi.org/10.1002/admi.201600805.
(10) Christov, N. C.; Danov, K. D.; Kralchevsky, P. A.; Ananthapadmanabhan, K. P.; Lips, A. Maximum Bubble Pressure Method: Universal Surface Age and Transport Mechanisms in Surfactant Solutions. *Langmuir* **2006**, *22* (18), 7528–7542. https://doi.org/10.1021/la061239h.
(11) Sakmann, B.; Neher, E. *Single-Channel Recording*, 2nd ed.; Sakmann, B., Neher, E., Eds.; Springer US: Boston, MA, 1995. https://doi.org/10.1007/978-1-4419-1229-9.
(12) Armstrong, C. M.; Chow, R. H. Supercharging: A Method for Improving Patch-Clamp Performance. *Biophys. J.* **1987**, *52* (1), 133–136.

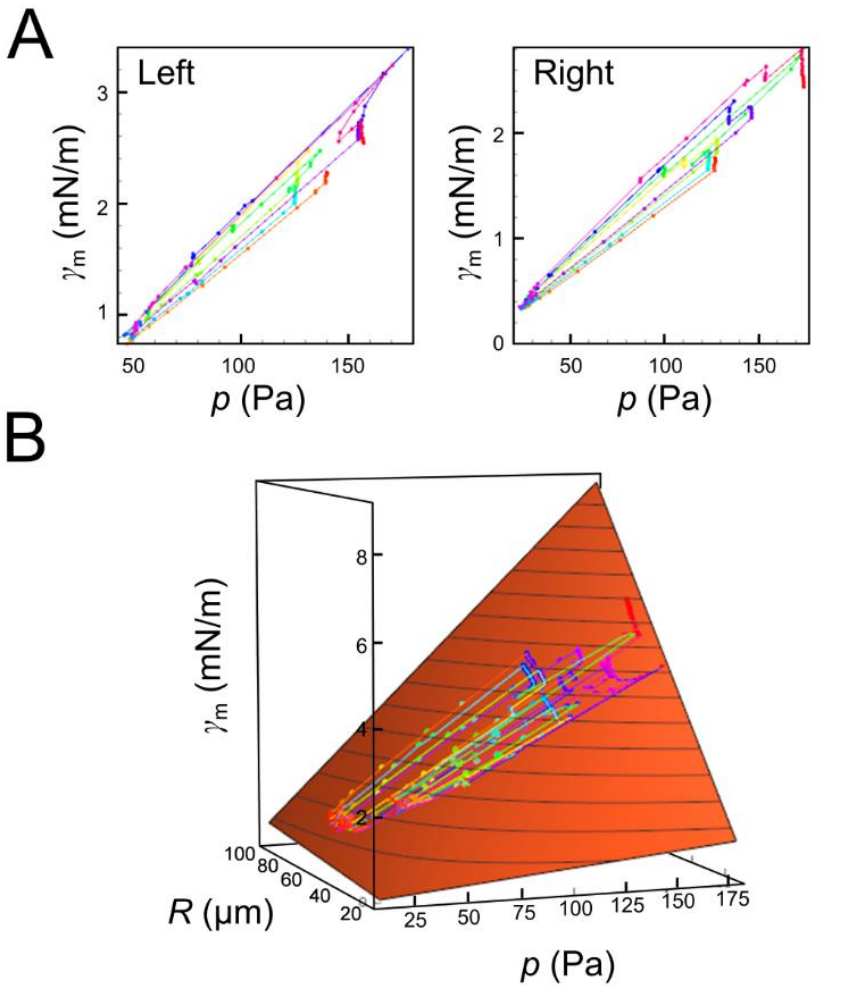

Figure S1. Relation between the intra-bubble pressure and monolayer tension. (A) γ_{mo} as a function of *p* for the left and right bubbles. (B) Trajectories projected on to the Young-Laplace plane in the three-dimensional plot. The slope of the γ_{mo}-*p* relation is not constant. However, projecting the monolayer tension data, as well as the radius data, onto the three-dimensional Young-Laplace surface, the different slopes are attributed to different sizes of the bubbles.

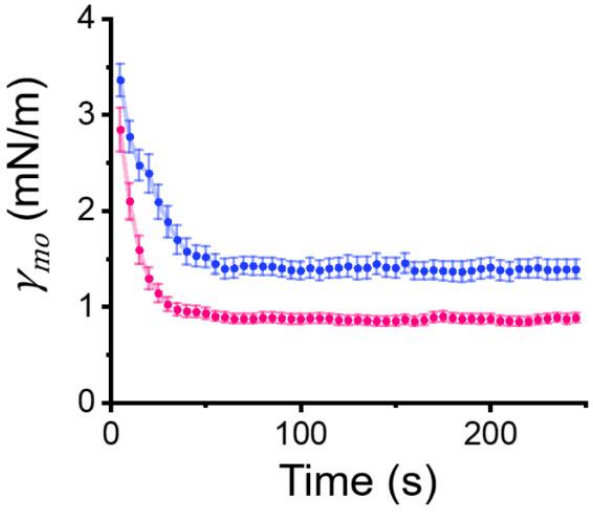

Figure S2. Time course of changes in tension for the azolectin monolayer. Liposome suspension solution was rapidly inflated from the tip of a glass pipet until the bubble diameter reaches approximately 100 μm (time zero). Since then, the bubble forming pressure was manipulated to keep the diameter constant under visual inspection. Pressure and bubble diameter were monitored, from which the monolayer tensions were analyzed every 5 sec using the Young-Laplace equation. Measurements were performed in the absence (blue) and presence (pink) of 3 mg/mL cholesterol in hexadecane.

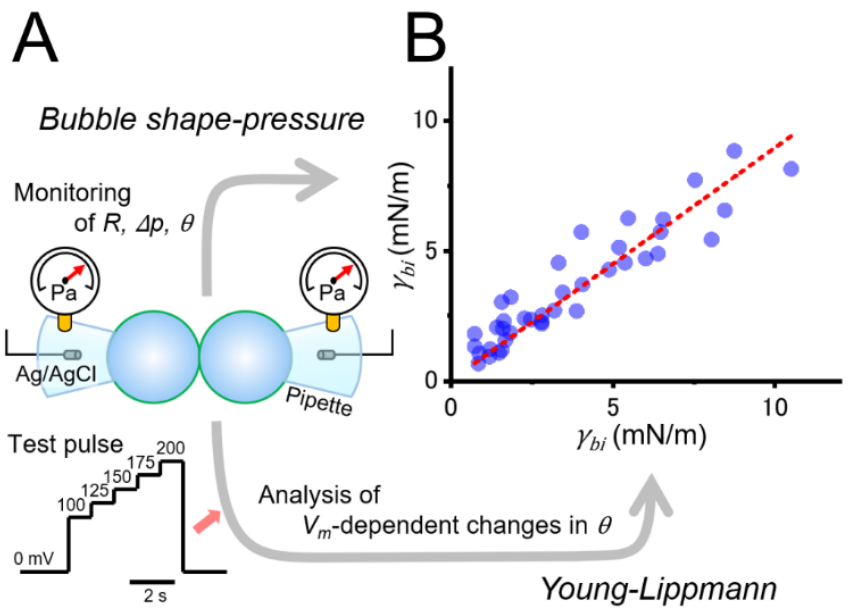

Figure S3. Comparison of lipid bilayer tension analysis using the bubble shape-pressure method and the voltage step method. (A) Schematic representation of the present bubble shape-pressure method utilizing the Young-Laplace principle and the previous voltage method utilizing the Young-Lippmann principle. For the voltage step method, five voltage steps are applied, and the membrane capacitance and contact angle in the steady state are measured. Thus, several seconds are needed to complete the step potential protocol, during which the single-channel current recordings are discontinuous. Thus, the tension and channel current evaluations are intermittent and alternating in the voltage step method. (B) Relation between the bilayer tension values analyzed by the two methods. The linear regression line is depicted as a broken red line.

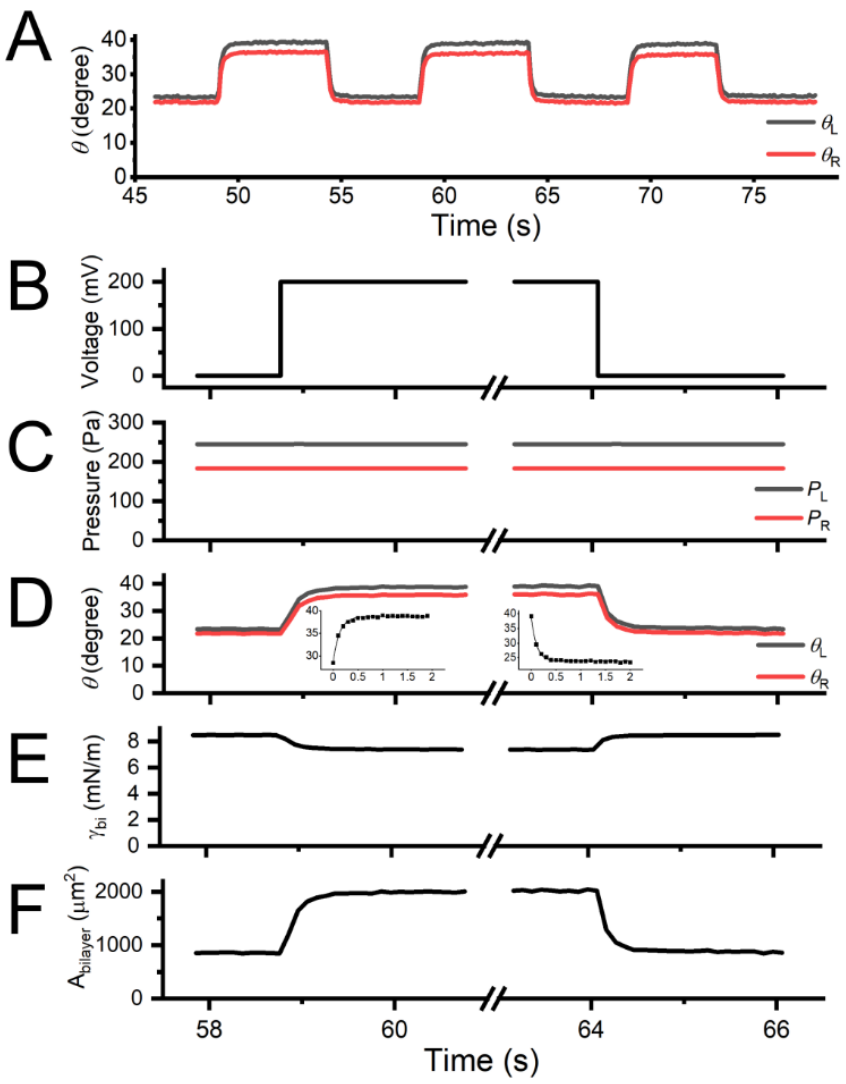

Figure S4. Dynamic responses of the contact angle upon a step changes in the membrane potential. (A) The membrane potential of +200 mV was repeatedly applied from 0 mV, and the contact angle for both sides is shown. (B-F) The time course of parameters with an expanded time scale. Upon a voltage step to +200 mV and return to 0 mV (B), the bubble pressure does not change (C). The contact angle rapidly changes (D), and the changing rate was faster upon return to the voltage. Inset shows changes in the contact angle (left bubble) and an exponential fit. The γ_{bi} value (E) follows a similar time course of the contact angle because the pressure is constant (the Young principle). The membrane area (F) is another independent parameter, representing zipping and unzipping, but shows a similar time course. The time constant (τ) for each parameter upon voltage application (+200 mV) was the followings: τ_{θ} = 173.1 ± 12.7 ms, $\tau_{\gamma bi}$ = 196.9 ± 12.9 ms, τ_{Abi} = 187.4 ± 12.8 ms. For the return to 0 mV: τ_{θ} = 115.4 ± 9.2 ms, $\tau_{\gamma bi}$ = 102.8 ± 8.7 ms, τ_{Abi} = 109.7 ± 9.0 ms (n = 8).

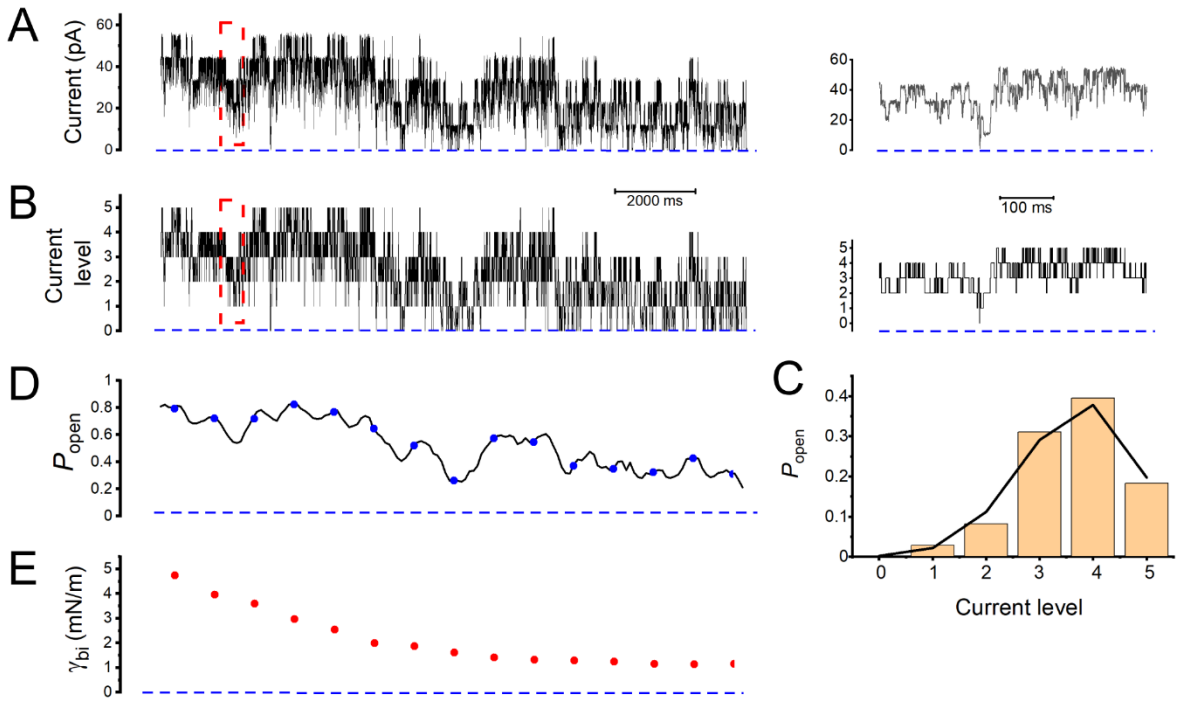

Figure S5. Analysis of the P_{open} and γ_{bi}. (A) The channel current trace, involving five active channels, retrieved from Figure 3C. Inset: A current trace in the boxed region in the left trace with an expanded time scale. (B) Digitalized current-level trace. The raw current trace was digitalized with an event-detecting program (Clampfit, Molecular Device). *Inset*: A current-level trace in the boxed region in the left trace with an expanded time scale. (C) A current-level histogram and fitting to the binomial distribution. The probability of each current level was calculated from a segment of the current level trace of 500 ms (bar graph), and the P_{open} was calculated as 0.786 by fitting to the binomial distribution (line graph). (D) Time course of P_{open} values. P_{open} was calculated every 100 ms along the whole current trace using the above method (solid line). P_{open} values at the instance of the image capture (1 Hz; E) are shown (Blue circle). (E) Time course of the γ_{bi} values. The γ_{bi} values are calculated from the geometrical parameters (sampling rate: 1 Hz) and the bubble pressure.

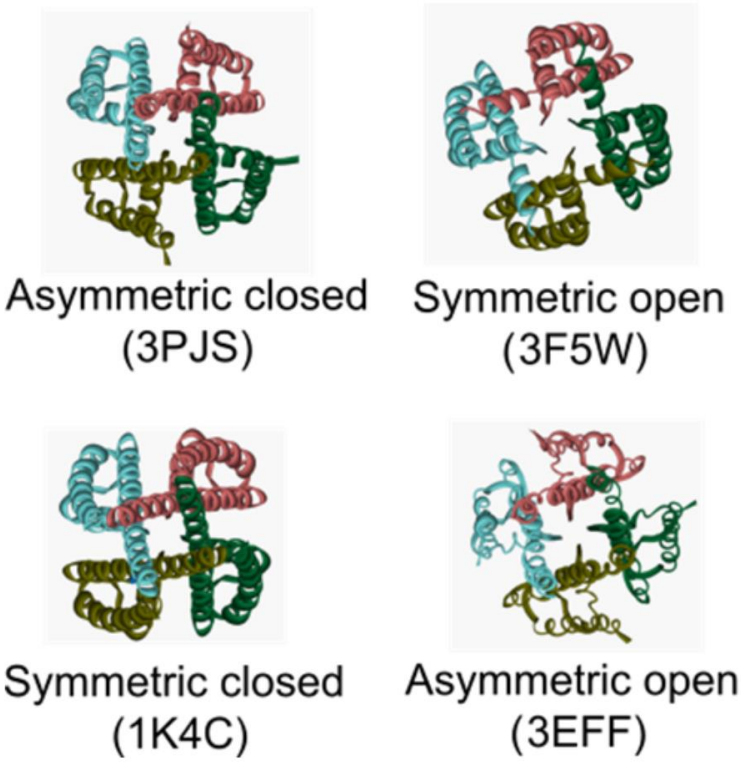

Figure S6. A Four different conformations of the KcsA channel crystal structure viewed from the cytoplasmic side. The cytoplasmic domain is truncated for the asymmetric conformations.